Geotechnical Testing Journal, Vol. 26, No. 3
Paper ID GTJ10783_263
Available online at: www.astm.org

Yu-Hsing Wang,[1] *Giovanni Cascante,*[2] *and J. Carlos Santamarina*[3]

Resonant Column Testing: The Inherent Counter EMF Effect

ABSTRACT: The standard magnet-coil driving system in resonant column devices provides the required cyclic excitation; however, it inherently produces a counter electromotive force that opposes the motion. In this study, the resonant column is modeled as an electro-mechanical system to quantitatively examine the counter electromotive effect and to explore its effect on resonant frequency and damping ratio computed from voltage-based measurements. The model is verified with two independent sets of experiments. Experimental and analytical results show that the measurement bias is more pronounced on the damping ratio than on the resonant frequency, the damping bias is not a device constant but varies with frequency, and the error is particularly relevant in low-loss and low-stiffness specimens (such as dry sands at low confinement). The electro-mechanical model permits developing device-specific correction charts that can be used to reexamine previously published damping ratio data gathered with voltage-based resonant column procedures.

KEYWORDS: resonant column testing, EMF effect, magnet-coil driving system

The resonant column technique has been extensively used for dynamic soil characterization in geotechnical laboratories since the 1960s (Wilson and Dietrich 1960; Hardin and Richart 1963; Hardin and Music 1965). The evolution of resonant column devices and techniques has involved testing in a wide strain range at various confining pressure and stress anisotropy conditions (Drnevich et al. 1978; Stokoe and Lodde 1978; Isenhower 1980; Alarcon et al. 1986; Isenhower et al. 1987; Kim et al. 1991; Ampadu and Tatsuoka 1993; Hardin et al. 1994; Cascante and Santamarina 1997), broad band frequency excitation through feedback vibration methods and virtual mass, and effective random noise excitation at very small strain levels (Li et al. 1998; Cascante and Santamarina 1996). A comprehensive review of the earlier developments can be found in Woods (1994).

The resonant column testing technique has been standardized (ASTM D 4015). It is considered a nondestructive test when measurements are conducted at strains below the elastic threshold strain for the soil under consideration at the given stress level. In this regime, the test is used to determine the maximum shear modulus G_{max} and the minimum damping ratio D_{min}.

Several potential testing biases inherent in the resonant column technique have been studied including: the number of cycles (Drnevich and Richart 1970; Kim et al. 1991), coupling between the specimen and the end platens (Drnevich 1978), the influence of end restraints (Yu and Richart 1984; Ashmawy and Drnevich 1994), membrane effects (Drnevich 1985), and energy leakage to the pedestal on the resonant column base (Drnevich 1978; Avramidis and Saxena 1990). In general, these effects are small at small-strain levels (say $\gamma \leq 10^{-5}$) and at typical resonant frequencies attained in near-surface soil studies.

Received August 27, 2001; accepted for publication September 18, 2002; published August 13, 2003.

[1] Assistant professor, Civil Engineering, Hong Kong University of Science and Technology, Hong Kong.
[2] Associate professor, Civil Engineering, University of Waterloo, Waterloo, ON N2L 3G1, Canada.
[3] Professor, Civil and Environmental Engineering, Georgia Institute of Technology, Atlanta, GA 30332.

Another inherent effect in standard resonant column systems is related to the source. The resonant column is excited with magnet-solenoid pairs. The relative displacement between the magnets and solenoids changes the magnetic flux passing through the coils and renders an electromotive force (EMF) that opposes the motion. This inherent counter-excitation introduces a complex impedance to the electro-mechanical device-specimen system. This effect has been noticed for decades beginning with Hardin, who considered using the counter EMF effect to monitor the excitation of the column in lieu of transducers. While ASTM D 4015 properly indicates the measurement of current in resonant column testing (Cascante et al. 2002; Meng and Rix 2002), it appears that most published results are based on the applied and measured voltage. Kim et al. (1991) correct the damping ratio computed with voltage by subtracting the damping ratio obtained with a calibration metal specimen whose inherent material damping is assumed null. Li et al. (1998) present detailed discussions and correct counter EMF through a sensitive control system. Still, the extent of this bias remains unclear. The purposes of this study are to examine this effect in detail, to develop a comprehensive electro-mechanical model for the resonant column, and to verify it with a unique set of experiments.

Electromechanical Model of the Resonant Column Device

The Induced Counter Electromotive Force

The driving cyclic torque in the resonant column device is generated through the interaction between the magnetic fields generated by the magnets and the solenoids. Consider a magnet-solenoid pair. When a current i runs through the solenoid, the magnetic field B that is generated is

$$B = \mu_0 \cdot n \cdot i \tag{1}$$

where μ_0 is the permeability of the free space, and n is the number of loops per unit length. The force F exerted onto the magnet is proportional to the magnetic field B; therefore, to the current i (from

Eq 1),

$$F = k_1 \cdot i \tag{2}$$

where k_1 is a proportionality constant. On the other hand, the movement of a magnet inside a coil induces counter EMF the coil. According to Faraday's law of induction,

$$V_{emf} = N \cdot \frac{d\Phi_B}{dt} \tag{3}$$

where N is the number of wire loops and Φ_B is the magnetic flux caused by the magnet across the cross-sectional area of the loops. This equation can be written in terms of the relative velocity (v) between the magnet and the coil. The linearization for small relative displacements renders,

$$V_{emf} = k_2 \cdot v \tag{4}$$

where k_2 is a proportionality constant.

The coil can be considered as an inductor L in series with a resistance R. Then, the impedance of the coil Z_{coil} is

$$Z_{\text{coil}} = R + j\omega L \tag{5}$$

where ω is the applied angular frequency and $j = \sqrt{-1}$. Combining Eqs 2, 4, and 5, the force from the induced counter EMF is

$$\begin{aligned} F_{emf} = k_1 \cdot i_{emf} = k_1 \cdot \frac{V_{emf}}{Z_{coil}} = k_1 \cdot \frac{V_{emf}}{R + j\omega L} = \frac{k_1 \cdot k_2 \cdot v}{R + j\omega L} \\ = \left[\frac{k_1 \cdot k_2 \cdot R}{R^2 + \omega^2 L^2} - j \frac{k_1 \cdot k_2 \cdot \omega \cdot L}{R^2 + \omega^2 L^2} \right] \cdot v \end{aligned} \tag{6}$$

The imaginary part represents a component out of phase, and it plays the role of a "virtual inertia" (note that $v \cdot \omega$ is acceleration). Thus, the counter force has in-phase and out-of-phase components and both are frequency dependent.

Electro-Mchanical Model

Consider the specimen in the resonant column as a linear viscoelastic material (Voigt model; the same assumption is made in ASTM D 4015). For a fixed-base resonant column system, the force balance equation including the counter electromotive torque is

$$I_t \cdot \ddot{\phi} + c_{soil} \cdot \dot{\phi} + K_t \cdot \phi = T_0 \cdot e^{j\omega\omega} - T_{emf} \tag{7}$$

where I_t is the rotational moment of inertia of the system, the soil column plus the driving head, ϕ, $\dot{\phi}$ and $\ddot{\phi}$ are the angular displacement, velocity, and acceleration, c_{soil} is the lumped viscosity for the soil column, K_t is the torsional stiffness, ω is the applied angular frequency, $T_0 \cdot e^{j\omega t}$ is the applied torque, and T_{EMF} is the torque caused by the induced EMF from Eq 6. Equation 7 is the electromechanical model of the resonant column device and takes into consideration the counter EMF. Substituting Eq 6 into Eq 7,

$$\begin{aligned} I_t \cdot \ddot{\phi} + c_{soil} \cdot \dot{\phi} + K_t \cdot \phi + \frac{\alpha \cdot \beta \cdot \phi \cdot R}{R^2 + \omega^2 L^2} \\ - j \frac{\alpha \cdot \beta \cdot \dot{\phi} \cdot \omega L}{R^2 + \omega^2 L^2} = T_0 \cdot e^{j\omega t} \end{aligned} \tag{8}$$

where, in this case, the proportionality constants α and β correspond to $V_{emf} = \alpha \cdot \phi$, and $T = \beta \cdot i \cdot k_1$, k_2, and v in Eq 6 are replaced by α, β, and ϕ, while the torque T_{EMF} is considered instead of force F_{EMF}. Rearranging Eq 8,

$$\begin{aligned} \left(I_t - \frac{\alpha \cdot \beta \cdot L}{R^2 + \omega^2 L^2} \right) \cdot \ddot{\phi} \\ + \left(c_{soil} + \frac{\alpha \cdot \beta \cdot R}{R^2 + \omega^2 L^2} \right) \cdot \dot{\phi} + K_t \cdot \phi = T_0 \cdot e^{i\omega t} \end{aligned} \tag{9}$$

$$(I_t - I_{EMF}) \cdot \ddot{\phi} + (c_{soil} + C_{EMF}) \cdot \dot{\phi} + K_t \cdot \phi = T_0 \cdot e^{i\omega t} \tag{10}$$

It follows from this equation that the "virtual inertia" I_{EMF} is

$$I_{EMF} = \frac{\alpha \cdot \beta \cdot L}{R^2 + \omega^2 L^2} \tag{11}$$

and the additional electrical damping in the system c_{EMF} is

$$c_{EMF} = \frac{\alpha \cdot \beta \cdot R}{R^2 + \omega^2 L^2} \tag{12}$$

Hence, the induced counter EMF increases both the measured damping ratio and the measured resonant frequency.

Experimental Observations

Preliminary Confirmation

The counter EMF effect can be readily studied by testing a calibration aluminum specimen (diameter 1.9 cm, height 23 cm, held with screws) in a special resonant column device that permits removing the coils. Three different tests are implemented including free vibration decay without coils, free vibration decay with coils-in-open, free vibration decay with coils-in-short (ends are connected together). The initial quasi-static torque is generated by a 0.5-mm pencil lead that eventually breaks, freeing the system into free vibration (Glaser et al. 1998).

Test results are shown in Fig. 1. The following observations can be made. First, the measured values of damping ratio are identical when tests are run without coils and with coils-in-open. Second, a much higher damping ratio is measured with coils-in-short (about five times higher in this case). Third, there are only small differences in resonant frequency; in particular, the resonant frequencies measured without coils and with coils in open exhibit a discrepancy smaller than 0.09 %. These results are further explored in the following series of tests.

Different Specimens and Excitation Modes

For this study, the four coil-magnet pairs in the standard torsional-resonant column (SBEL Stokoe D1128) are reconnected into two sets, A and B, which can work individually, as shown in Fig. 2 (note that the two coils in each set are connected in series). This configuration permits running six different tests:

(1) Free vibration decay with all coils in open.
(2) Free vibration decay with the A set in-short and the B set in-open.
(3) Free vibration decay with coils in both A and B sets in-short.
(4) Resonant, forced excitation driven by coils in the A set, while coils in the B set are left in-open.
(5) Resonant excitation driven by coils in both A and B sets, connected in parallel.
(6) Resonant excitation driven by all coils, both sets A and B connected in series.

Given that identical results are obtained in free vibration decay without coils or with coils in open (as shown in Fig. 1), test results

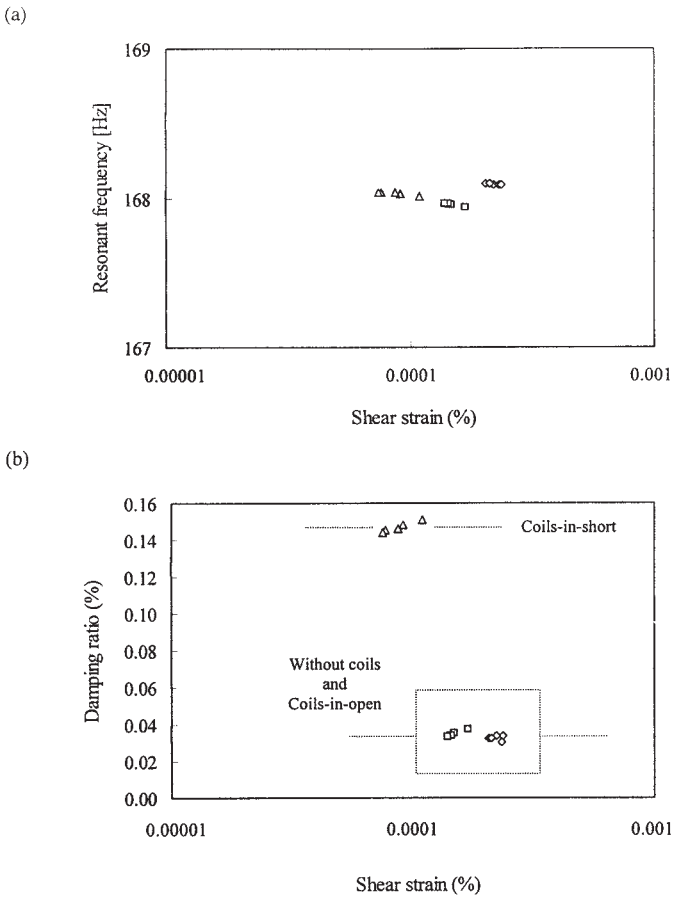

FIG. 1—*Results of free vibration decay test implemented in a column that permits removing the coils: (a) resonant frequency; (b) damping ratio; symbols: ◇ = without coils, □ = coils-in-open, Δ = coils-in-short.*

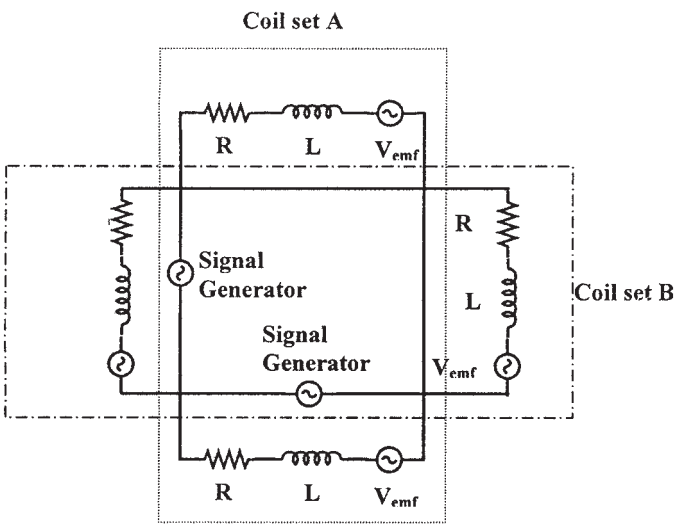

FIG. 2—*Equivalent circuits for the regrouped coil sets.*

obtained with the first procedure are considered the "true values." Note that, in this study, the term "true" refers to measured parameters that are not affected by counter EMF effects. However, other biases may still affect the "true" values documented herein, including radiation at the base of the specimen. As a reference, the

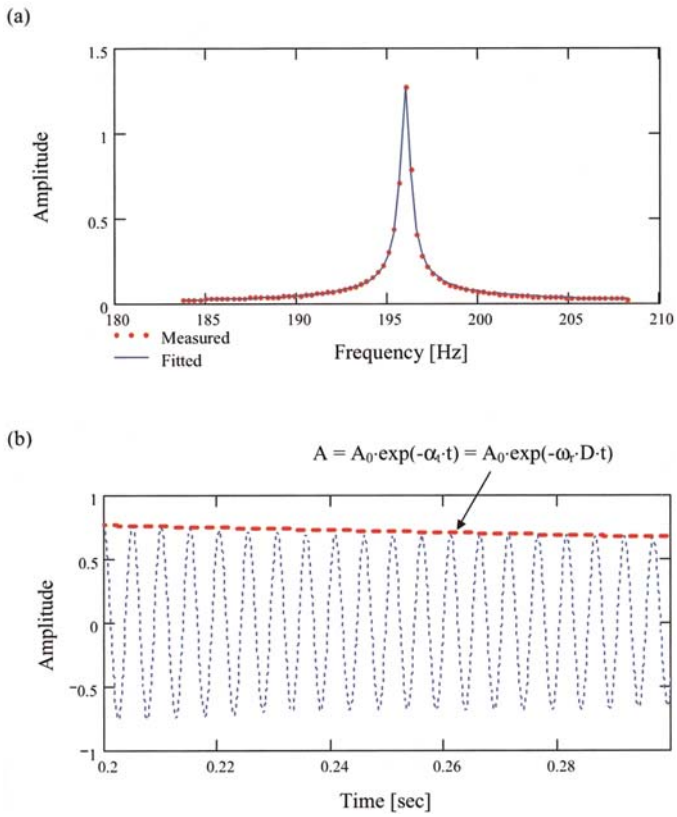

FIG. 3—*Results of free vibration decay with coils in open (Aluminum Specimen I): (a) frequency response function; (b) time series.*

damping ratio of aluminum can be as low as $D = 2.5 \times 10^{-6}$ (frequency range 1 to 200 kHz—Zemanek and Rudnick 1961).

The damping ratio and the resonant frequency in *free vibration decay* tests are obtained by curve fitting the acceleration frequency response (the Fourier transform of the free vibration decay time records—approximately 150 ~ 600 cycles are captured in each time series). A digital storage oscilloscope (Rapid System 2000) is used to collect time records. Figure 3 shows the time domain and the frequency domain responses fitted with the same damping ratio.

Resonant excitation tests are implemented using the random noise excitation technique (Cascante and Santamarina 1997). Given the low impedance of signal generators, coils that are connected to signal generators produce the same counter electromotive effect as coils in short. The damping ratio and the resonant frequency are obtained from the stored frequency response obtained from the signal analyzer (Network signal analyzer, Model SR780, Standford Research System) by curve fitting the theoretical response in terms of "acceleration/input voltage" to capture the counter EMF effect.

Three aluminum specimens with very different resonant frequencies are used in this study. The properties for the three specimens are listed in Table 1. Test results obtained for the six different test procedures with the three aluminum specimens are summarized in Figs. 4, 5, and 6, and in Table 2. The following observations can be made. First, the measured damping ratio and resonant frequency increase with increasing number of coils in short. Second, as shown before, the counter EMF affects the damping ratio more than the resonant frequency. Third, the measurement bias

TABLE 1—*Properties of the three aluminum specimens tested in this study.*

Specimens	Unit Weight, g/cm^3	Weight, g	Outside Diameter, cm	Inside Diameter, cm	Length, cm	Moment of Inertia, kg·cm^2	Nominal Resonant Frequency, Hz
Aluminum I	2.77	345.8	2.540	1.900	13.98	1.579	196
Aluminum II	2.77	258.4	2.540	2.354	13.94	1.484	123
Aluminum III	2.77	42.2	0.796	0.528	20.45	0.130	19

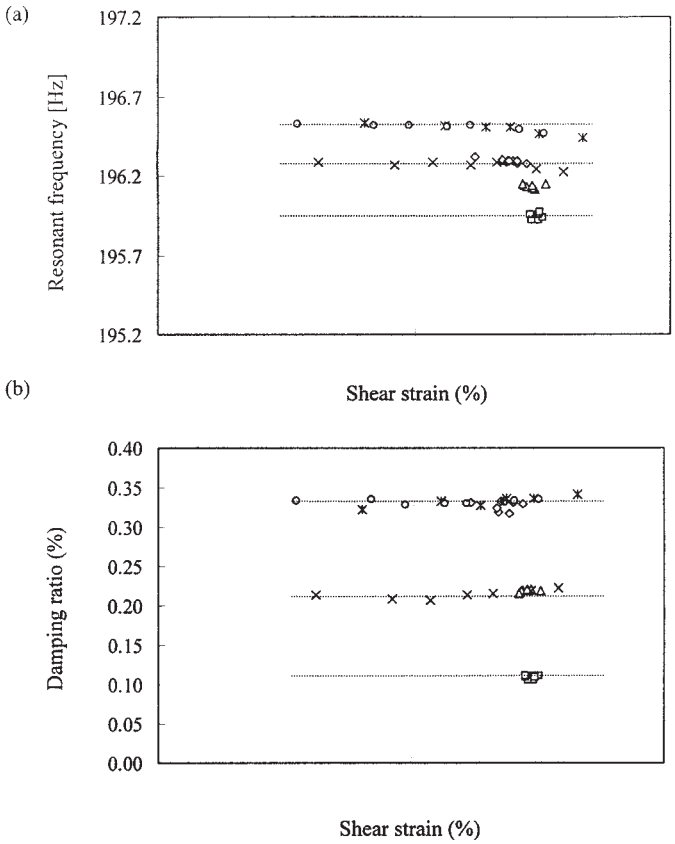

Symbols	Test Types	Coil Connections	
		Set A	Set B
	Free Vibration Decay	Open	Open
Δ	Free Vibration Decay	Short	Open
*	Free Vibration Decay	Short	Short
x	Resonant Excitation	Short (drive)	Open
◊	Resonant Excitation (Sets A and B in parallel)	Short (drive)	Short (drive)
o	Resonant Excitation (Sets A and B in series)	Short (drive)	Short (drive)

FIG. 4—*Test results with Aluminum Specimen I: (a) resonant frequency; (b) damping ratio (note: driving coils are effectively in short).*

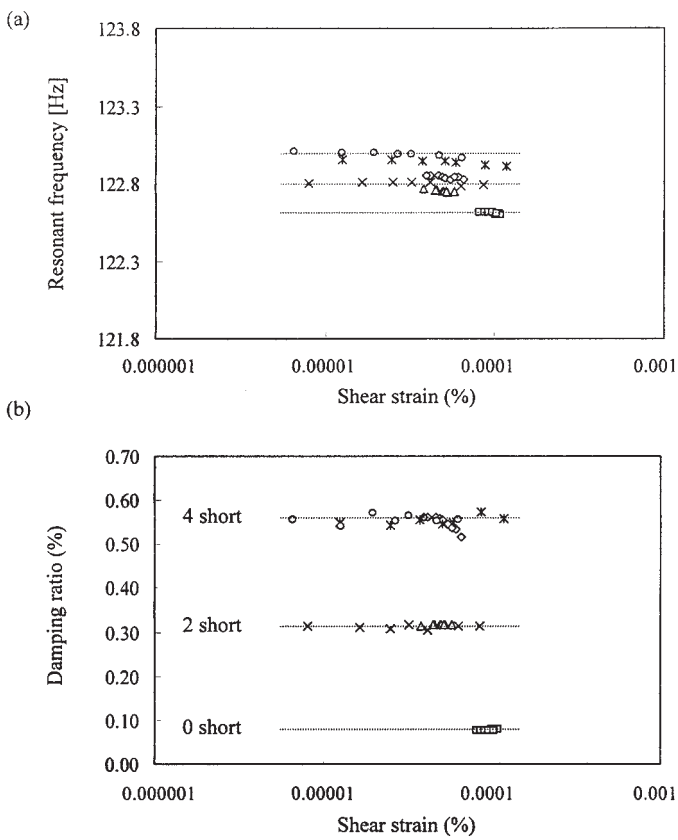

Symbols	Test Types	Coil Connections	
		Set A	Set B
	Free Vibration Decay	Open	Open
Δ	Free Vibration Decay	Short	Open
*	Free Vibration Decay	Short	Short
x	Resonant Excitation	Short (drive)	Open
◊	Resonant Excitation (Sets A and B in parallel)	Short (drive)	Short (drive)
o	Resonant Excitation (Sets A and B in series)	Short (drive)	Short (drive)

FIG. 5—*Test results with Aluminum Specimen II: (a) resonant frequency; (b) damping ratio (note: driving coils are effectively in short).*

increases with decreasing resonant frequency, as summarized in Fig. 7. Note that the measured damping ratio is about 40 times higher than the "true" damping ratio for the low-resonant-frequency Aluminum Specimen III. Fourth, measured damping ratios using free vibration decay and resonant excitation are similar for two coils in short/drive (Procedures 2 and 4) and for four coils in short/drive (Procedures 3 and 5 or 6). These results are used to validate the electro-mechanical model described above. Ultimately, the model must be able to predict results gathered with the six different test sequences and explain these observations.

Model Parameters-Predictions-Validation

Model Parameters—Measurement

Resistance R and Inductance L—Four parameters, *R*, *L*, α, and β are needed to evaluate the electro-mechanical model (Eq 9). The resistance *R* and the inductance *L* of the coils are measured with an impedance analyzer in a broad frequency range (Hewlett- Packard 4192 A). The measured resistance *R* and inductance for either Set A or Set B are $R = 22.28\ \Omega$ and $L = 12.43 \cdot 10^{-3}$ H. These values apply across the operating frequency of the resonant column.

Proportionality Factor α ($V_{EMF} = \alpha \cdot \dot{\phi}$)—The α factor is quantified by exciting coil Set A with a sinusoidal signal and measuring the potential induced by the displacement of the magnets in coil Set B (at 123 Hz). The schematic diagram of the setup is shown in Fig. 8. The angular velocity of the coils is measured with the accelerometer, which is mounted on the driving system. Results are shown in Fig. 9. The value of α for one coil set is α = 0.543 V/rad/s. There is a very small velocity-dependent phase lag between the generated voltage and the movement of the coils (Fig. 9*b*). This imaginary component of α is disregarded in this analysis.

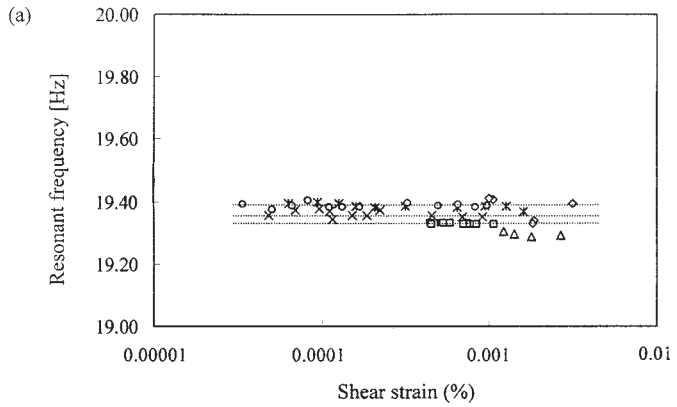

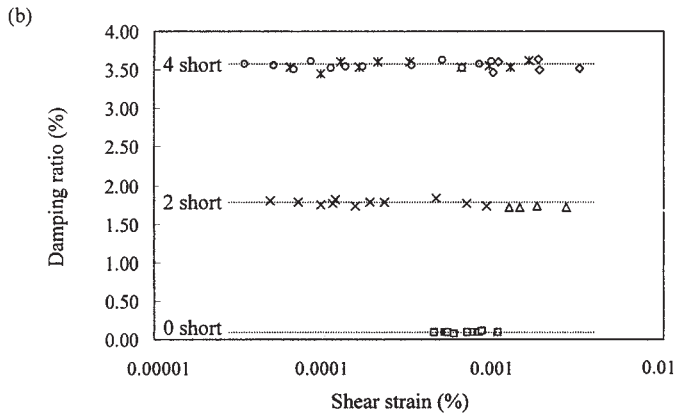

Symbols	Test Types	Coil Connections	
		Set A	Set B
	Free Vibration Decay	Open	Open
Δ	Free Vibration Decay	Short	Open
*	Free Vibration Decay	Short	Short
x	Resonant Excitation	Short (drive)	Open
◊	Resonant Excitation (Sets A and B in parallel)	Short (drive)	Short (drive)
o	Resonant Excitation (Sets A and B in series)	Short (drive)	Short (drive)

FIG. 6—*Test results with Aluminum Specimen III: (a) resonant frequency; (b) damping ratio (note: driving coils are effectively in short).*

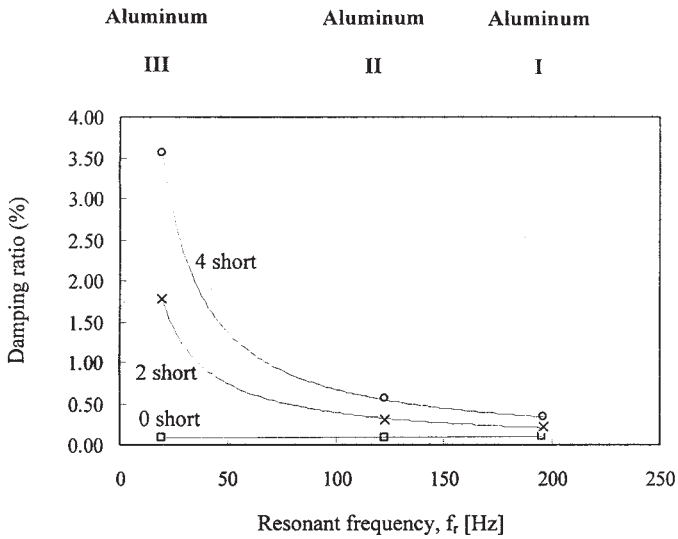

Symbols	Test Types	Coil Connections	
		Set A	Set B
□	Free Vibration Decay	Open	Open
x	Resonant Excitation	Short (drive)	Open
o	Resonant Excitation (Sets A and B in series)	Short (drive)	Short (drive)

FIG. 7—*Summary of test results (average values are shown). The bias in damping ratio increases with decreasing resonant frequency and with increasing number of coils in-short (or used for driving the system).*

TABLE 2—*Test results—summary.*

Specimens	Parameters	FVD	FVD A in Short, B in Open	FVD A + B in Short	RC Driving with A, B in Open	RC Driving with A + B in Parallel	RC Driving with A + B in Series
Aluminum I	f_r (Hz)	195.94	196.14	196.29	196.27	196.49	196.50
	D (%)	0.109	0.219	0.328	0.214	0.333	0.331
Aluminum II	f_r (Hz)	122.61	122.75	122.84	122.80	122.94	122.99
	D (%)	0.077	0.316	0.549	0.312	0.554	0.555
Aluminum III	f_r (Hz)	19.33	19.30	19.38	19.36	19.39	19.39
	D (%)	0.087	1.721	3.544	1.782	3.558	3.558

NOTE: FVD = free vibration decay; RC = resonant clumn testing; *fr* = resonant frequency; *D* = damping ratio.

Proportionality Factor β *(T = β·i)*—A torque transducer (Futeck model T5101) is used to quantify the proportionality constant β between the torque T and the current i for different coil-set connections (at 1 Hz). Results for one coil set are shown in Fig. 10. The input current is derived from the input voltage, since the values of R and L for the coils are known.

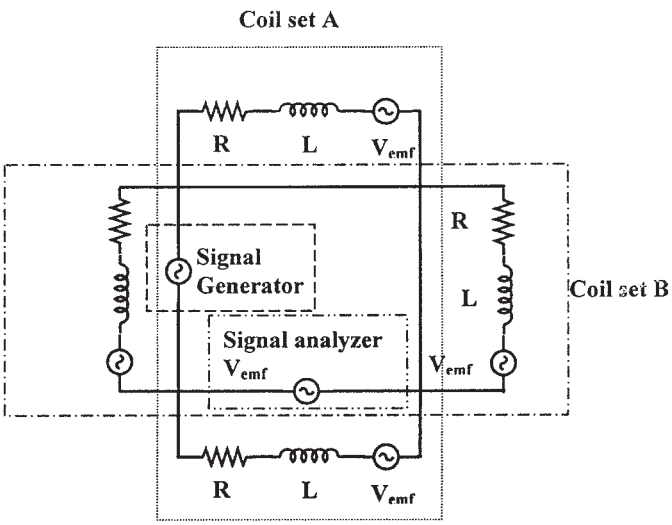

FIG. 8—*Schematic diagram of the setup for measuring* α.

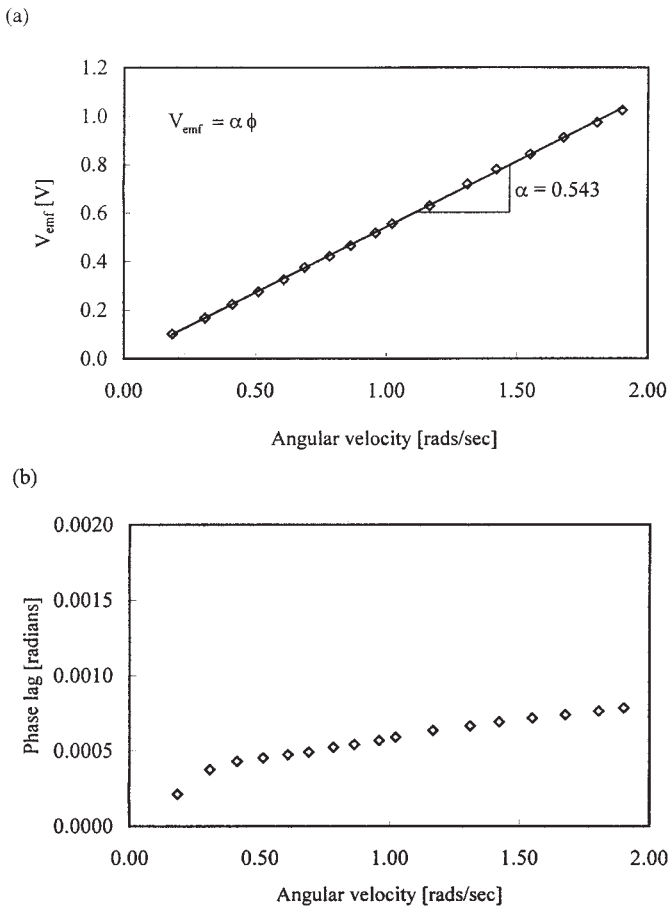

FIG. 9—*(a) Relationship between the counter voltage V_{EMF} and the angular velocity* ϕ *for one coil Set B; (b) the phase lag between V_{EMF} and* ϕ *versus angular velocity.*

Although a non-zero phase lag between *T* and *i* is detected, it is within the range of the hysteresis in the torque transducer, which is about 0.2%. Once again, only the real component of β is considered in the analysis.

Summary—Table 3 summarizes the values of α, β, *R*, and *L* for different coil-set combinations. Notice that α and β have not only the same units but approximately the same values as well. In fact, on the bases of causality, it is expected that α = β. Both values are retained in subsequent sections to facilitate the discussion.

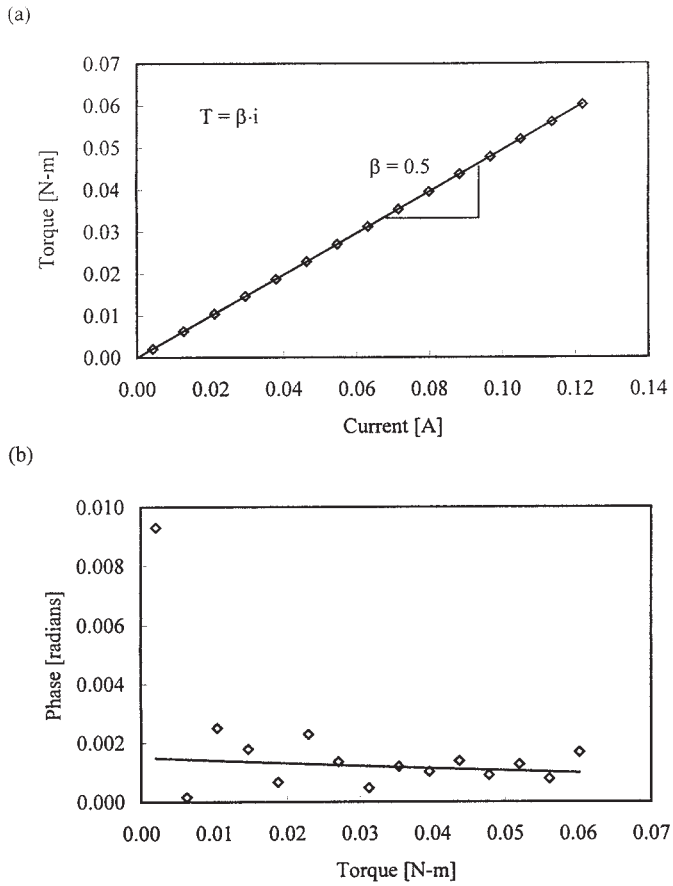

FIG. 10—*(a) Proportionality between torque T and input current i for coil set A; (b) phase lag between T and i versus torque.*

TABLE 3—*Summary of model parameters.*

Parameters	Coil Sets		
	A Set Only	A and B Coil Sets in Parallel	A and B Coil Sets in Series
System α (Voltage/rad/s)	0.543	[a]0.543	[a]0.543 × 2
System β (N-m/Ampere)[b]	0.5	0.5	1.0
R (Ohms)	22.28	22.28/2	22.28 × 2
L (10^{-3} Henrys)	12.43	12.43/2	12.43 × 2

[a] Computed/inferred.
[b] Input current (at the signal generator).

Model Predictions

Resonant Frequency—The counter EMF effect decreases the moment of inertia (Eq 10). Therefore, an increase in the measured resonant frequency is expected. Test results in Figs. 4 through 6 confirm this prediction. The normalized bias in resonant frequency can be estimated as

$$\frac{\omega_{rm} - \omega_{rt}}{\omega_{rt}} = \sqrt{\frac{I_t}{I_t - I_{emf}}} - 1 = \sqrt{\frac{I_t}{I_t - \dfrac{\alpha \cdot \beta \cdot L}{R^2 + \omega_{rm}^2 L^2}}} - 1 \quad (13)$$

where ω_{rm} and ω_{rt} are the measured and the true resonant frequencies, I_t is the true rotational moment of inertia, and I_{EMF} is the contribution from the counter EMF. When Eq 13 is evaluated for the measured model parameters, the predicted bias in resonant frequency is about 0.2 ~ 0.3 %. This small measurement error can be ignored for all practical purposes.

Damping Ratio—It follows from Eq 10 that the measured damping ratio D_m is

$$D_m = \frac{c_{soil} + c_{emf}}{2 \cdot I_m \cdot \omega_{rm}} \quad (14)$$

where I_m is the effective inertia and equal to $(I_t - I_{EMF})$. On the other hand, the true damping ratio D_t is

$$D_t = \frac{c_{soil}}{2 \cdot I_t \cdot \omega_{rt}} \quad (15)$$

Substituting c_{soil} from Eq 14 into 15, and solving for the true damping ratio D_t,

$$D_t = \frac{D_m \cdot 2 \cdot I_m \cdot \omega_{rm} - c_{emf}}{2 \cdot I_t \cdot \omega_{rt}} \quad (16)$$

Recognizing that I_t and ω_{rt} are very similar to I_m and ω_{rm}, the true damping ratio can be expressed in terms of measured parameters

$$D_t \approx D_m - \frac{\alpha \cdot \beta \cdot R}{R^2 + \omega_{rm}^2 L^2} \cdot \frac{1}{2 \cdot I \cdot \omega_{rm}} = D_m - D_{emf} \quad (17)$$

D_{EMF} is not an equipment constant, but varies with the resonant frequency.

Other Observation—The damping ratio contributed by the counter EMF in a set of coils (for example, A) is (from Eq 17; the other set is assumed open),

$$D_{emf,A} = \frac{\alpha_A \cdot \beta_A \cdot R}{R^2 + \omega_{rm}^2 L^2} \cdot \frac{1}{2 \cdot I_m \cdot \omega_{rm}} \quad (18)$$

where R and L are the resistance and inductance for a set of two coils. If the two sets of coils, A and B, are connected in parallel ("*ABp*"), the impedance of the combined coils halves, the values of constants α and β for the system, are the same as for coil Set A, and the electrical damping becomes:

$$D_{emf,ABp} = \frac{\alpha_A \cdot \beta_A \cdot R}{\frac{1}{2}(R^2 + \omega_{rm}^2 L^2)} \cdot \frac{1}{2 \cdot I_m \cdot \omega_{rm}} \quad (19)$$

On the other hand, the connection of the two sets, A and B, in series ("ABs") doubles the electrical impedance and the values of α and β (see Table 3), hence,

$$D_{emf,ABs} = \frac{2\alpha_A \cdot 2\beta_B \cdot R}{2(R^2 + \omega_{rm}^2 L^2)} \cdot \frac{1}{2 \cdot I_m \cdot \omega_{rm}} \quad (20)$$

Equations 18, 19, and 20 suggest that

$$D_{emf,ABs} = D_{emf,ABp} = 2 \cdot D_{emf,A} \quad (21)$$

Therefore, the electro-mechanical model predicts that the damping ratio from the induced EMF is proportional to the number coil sets in short (or connected to the signal generator).

Model Validation

The adequacy of the proposed electro-mechanical model of the resonant column is assessed herein. Voltage-based damping data are first corrected using the model formulation, i.e., Eq 17. Then model predictions are tested by gathering damping data with two and four coils.

Validation by Model-Based Correction—This validation was started with the measurement of the resistance R and the inductance L of the coils as connected in the resonant column (Table 3), and the determination of α and β (see Figs. 9 and 10). For the purposes of damping ratio correction, the effective inertia I_m was estimated as the true system inertia I_t, and the measured resonant frequency ω_{rm} was obtained from the frequency response. Finally, the corrected material damping ratio D_t was computed from the voltage-based measured value D_m by means of Eq 17.

The true damping ratio (measured in free vibration decay with open loops), and the damping ratio measured in resonant column tests (two different modes) before and after correction, are shown in Fig. 11. Values are summarized in Table 4 and corroborate the adequacy of the electro-mechanical model.

Prediction Verification: Self-healing Measurements—The measured damping ratio is the sum of the true damping ratio and the damping ratio from the counter EMF, as shown in Eq 17. Thus, the damping ratio measured in resonant column by driving the system with four or two coils are:

4 coils $\quad D_{m,4} = D_t + D_{emf,A}$ (series or parallel) (22)

2 coils $\quad D_{m,2} = D_t + D_{emf,2}$ (other two coils in open) (23)

Furthermore, Eq 21 shows that exciting the resonant column with four coils contributes a damping bias twice as high as exciting the column with two coils (and keeping the other two in open): $D_{EMF,\,4} = 2D_{EMF,\,2}$. Then, the true damping ratio of the material D_t can be computed from two measurements:

$$D_t = 2 \cdot D_{m,2} - D_{m,4} \quad (24)$$

This model prediction is verified by modifying the resonant column to accommodate an external switch that allows operating two coils (other two in-open) or exciting the four coils as prescribed in Fig. 8. Figure 12 and Table 5 show the measured, the true, and the corrected damping ratio values obtained by means of these self-healing, complementary measurements.

Observation: The Case of High Damping

The induced damping varies with the excitation frequency (Eq 12). Yet, the procedures outlined above presume a constant damping ratio near the resonant frequency. This assumption is valid when the true damping ratio of the specimen is low ($D < 0.05$).

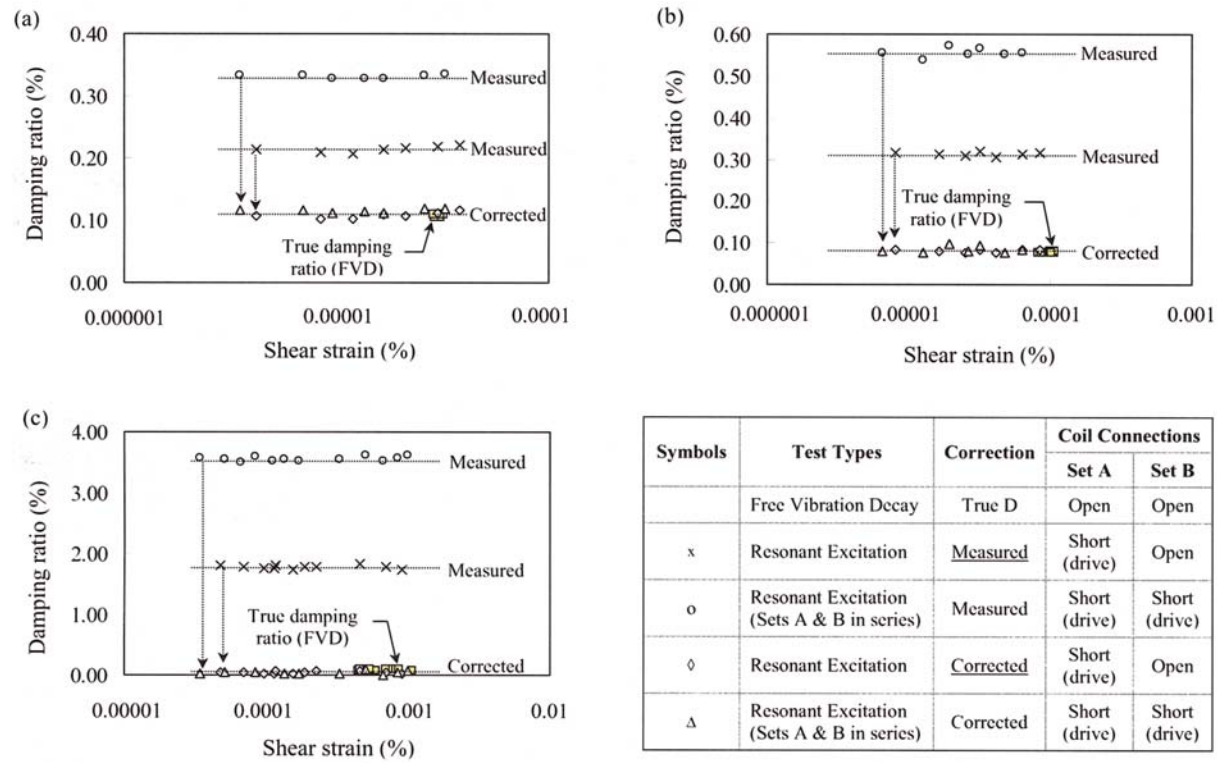

Symbols	Test Types	Correction	Coil Connections	
			Set A	Set B
	Free Vibration Decay	True D	Open	Open
x	Resonant Excitation	Measured	Short (drive)	Open
o	Resonant Excitation (Sets A & B in series)	Measured	Short (drive)	Short (drive)
◊	Resonant Excitation	Corrected	Short (drive)	Open
Δ	Resonant Excitation (Sets A & B in series)	Corrected	Short (drive)	Short (drive)

FIG. 11—*A comparison of the measured damping ratio before and after correction: (a) Aluminum Specimen I; (b) Aluminum Specimen II; (c) Aluminum Specimen III.*

TABLE 4—*Comparison between the measured true damping ratio and the damping ratio measured by RC tests before and after the model-based correction.*

	Test Types				
		RC Driving with A, B in Open		RC Driving with A + B in Series	
Specimens	FVD True Damping Ratio	Measured	Corrected	Measured	Corrected
Aluminum I	0.109 %	0.214 %	0.108 %	0.331 %	0.115 %
Aluminum II	0.077 %	0.312 %	0.081 %	0.555 %	0.084 %
Aluminum III	0.087 %	1.782 %	0.048 %	3.558 %	0.041 %

Note: "True" refers to measurements without counter EMF effect. Other non-materials losses may still be present, such as base radiation.

TABLE 5—*Comparison between the measured true damping ratio and the damping ratio corrected by self-healing complementary measurements.*

	Test Types			
Specimens	FVD True Damping Ratio	RC Driving with A, B in Open (Measure 1)	RC Driving with A + B in Series (Measure 2)	Complementary, Self-Healing Measurements, 2·(Measure 1) − (Measure 2)
Aluminum I	0.109 %	0.214 %	0.331 %	0.097 %
Aluminum II	0.077 %	0.312 %	0.555 %	0.069 %
Aluminum III	0.087 %	1.782 %	3.558 %	0.006 %

NOTE: "True" refers to measurement without counter EMF effect. Other non-materials losses may still be present, such as base radiation.

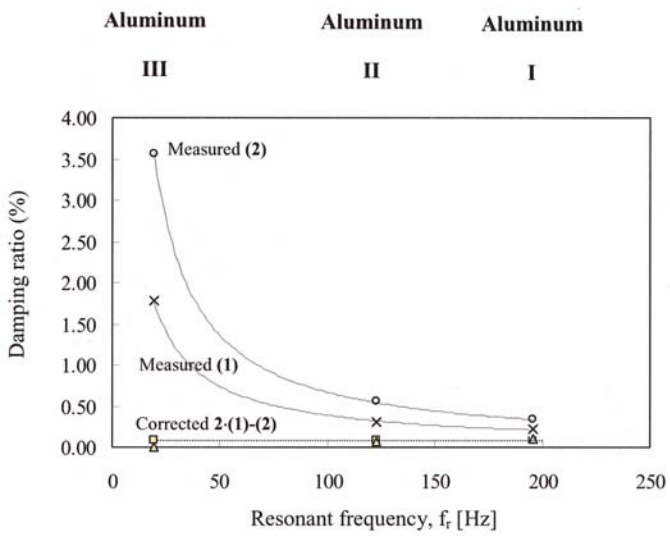

Symbols	Test Types	Coil Connections	
		Set A	Set B
□	Free Vibration Decay	Open	Open
x	Resonant Excitation (1)	Short (drive)	Open
o	Resonant Excitation (Sets A and B in series) (2)	Short (drive)	Short (drive)
△	Corrected by Complementary Measurement Method 2·(1)-(2)		

FIG. 12—*Measured damping ratio before and after correction by self-healing complementary measurements.*

However, as damping increases, the resonant peak becomes wider and is not uniformly affected by the induced counter EMF. In this case, Eq 17 gives an approximate correction for the measured damping ratio. The following quadratic equation is more appropriate for large damping ratios:

$$D_t^2 \cdot [R^2 + (\omega_{rt} L)^2] + D_t \left(\frac{R\alpha^2}{I_t \omega_{rt}} \right) - \left[\left(\frac{D_m \alpha r_a}{F_0} \right)^2 - \left(\frac{\alpha^2}{2 I_t \omega_{rt}} \right)^2 \right] = 0 \quad (25)$$

where F_0 is an amplification factor that depends on the mass and stiffness of the system, α is the proportionality constant ($V_{EMF} = \alpha \cdot \dot{\phi}$), and r_a is the distance from the accelerometer to the center of the specimen.

Relevance of RC Bias on Measured Material Parameters

Predicted Errors

As indicated earlier, the bias in the resonant frequency due to the counter EMF effect is very small and can be disregarded (Eq 13). On the other hand, the bias in voltage-based damping ratio contributed by the counter EMF effect can be significant. From Eq 17,

$$D_{emf} = \frac{\alpha \cdot \beta \cdot R}{R^2 + \omega_{rm}^2 L^2} \cdot \frac{1}{2 \cdot I_m \cdot \omega_{rm}} \quad (26)$$

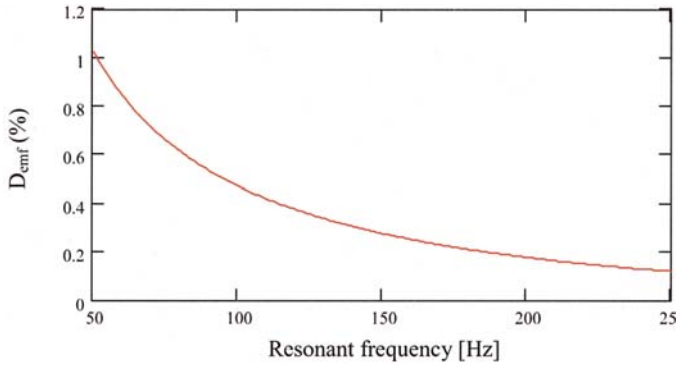

FIG. 13—*Estimated D_{EMF} for varying resonant frequencies based on Eq 26, where α = 1.0 V·rad^{-1}·sec^{-1}, β = 1.0 N·m/amp (Note that $\alpha = \beta$), R = 44.56 Ohms, L = 24.86 mH, I = 0.00338 kg·m^2 (driving with four coils).*

Using the equipment parameters measured earlier and choosing typical values for the moment of inertia, I_t (specimen 7.1 cm diameter, 13 cm height, and 852.46 g), the predicted D_{EMF} for four-coil excitation decreases with resonant frequency as shown in Fig. 13. Note that D_{EMF} is approximately equal to 1 % when the resonant frequency is $f \sim 50$ Hz. Thus, the voltage-based measured damping ratio may be dominated by the electromotive effect, particularly in dry soils at low confinement (low-resonant frequency).

The average value 0.4 % for the damping-ratio correction adopted by Kim et al. (1991) is close to the predicted D_{EMF} for a resonant frequency $f_r \sim 115$ Hz (Fig. 13).

Correction of Published Trends

These results highlight the need to reexamine previously published experimental results gathered with resonant column testing when the input voltage is used in the calculation of the transfer function. For example, results in Santamarina and Cascante (1996) for D_{min} gathered for air-dry sands (Barco Sand 32) at different confinement are plotted in Fig. 14*a*. Corrected results are also shown. It is concluded that the confinement dependence of D_{min} observed in Santamarina and Cascante (1996) is an artifact of the electromotive effect (Fig. 14*c*), whereby the measured (biased) damping ratio decreases with increasing the confinement (increasing the resonant frequency). Indeed, the confinement dependence of D_{min} vanishes after correction. Furthermore, the comparison of results before and after correction confirms that the measured damping ratio in dry sands at low confinement can be dominated by the counter-electromotive effect.

Conclusions

Counter electromotive effects in voltage-based resonant column measurements affect the measured resonant frequency and damping ratio. The bias in the measured resonant frequency can be ignored for most practical purposes. The bias on the measured damping ratio can be severe, particularly in low-loss materials (e.g., dry sand) at low- resonant frequency (i.e., low confinement).

The electro-mechanical model of the resonant column device adequately predicts experimental results. The damping ratio that results from the counter EMF effect is a function of the device characteristics and material properties, and it is algebraically additive to the material damping. It is not constant, but frequency dependent. The free vibration decay test with coils in open circuit renders the "true" material damping ratio unbiased by counter EMF effects.

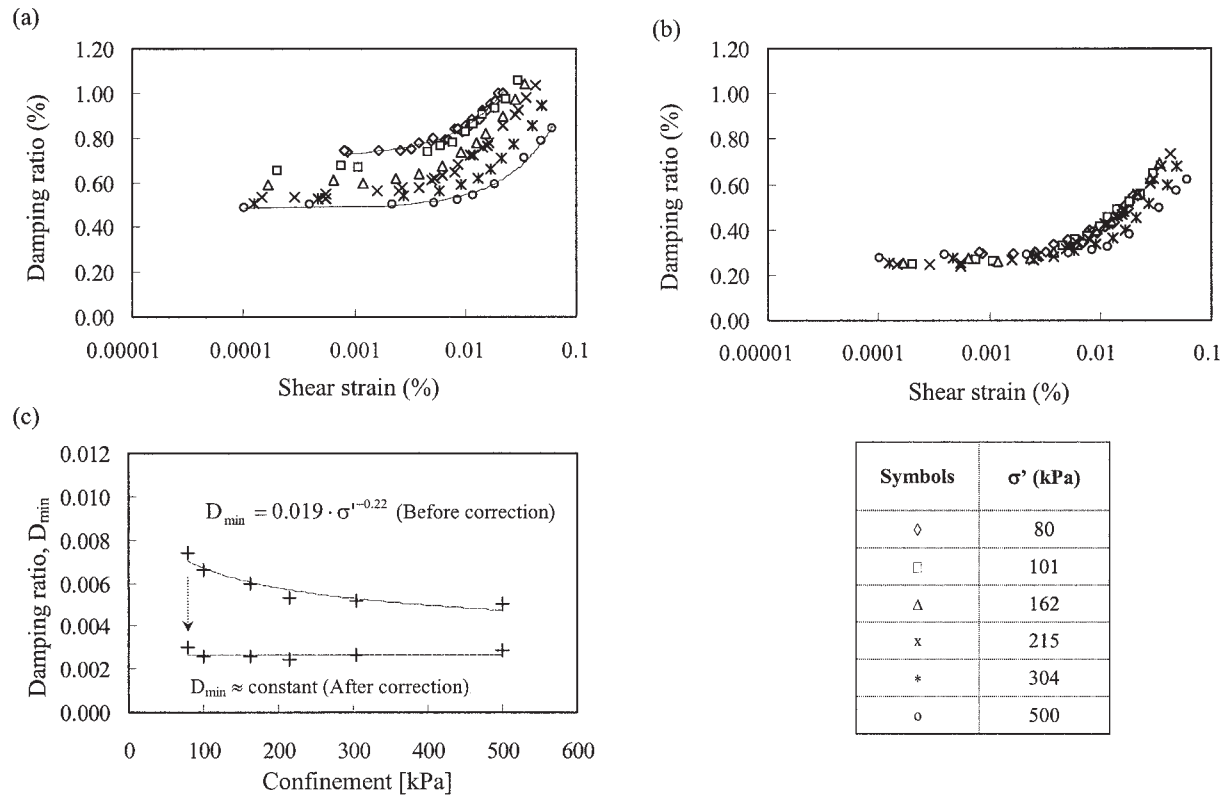

FIG. 14—*A comparison of published experimental results before and after correction for the counter EMF effect (air-dry sand): (a) before correction (four coil-magnet pairs are connected in series); (b) after correction; (c) the relation between confinement and D_{min} before and after correction (original data from Santamarina and Cascante, 1996).*

In view of this measurement bias, it is necessary to reexamine previously published experimental results based on voltage measurements and to reassess the conclusions they promoted.

Acknowledgments

This research was supported by grants from the NSF and the NSERC. The authors are grateful to Glenn Rix and Jeiwu Meng for insightful discussion during this research.

References

Alarcon, A., Chameau, J. L., and Leonards, G. A., 1986, "A New Apparatus for Investigating the Stress-Strain Characteristics of Sands," *Geotechnical Testing Journal,* Vol. 9, No. 4, pp. 204–212.

Ampadu, S. K. and Tatsuoka, F., 1993, "A hollow Cylinder Torsional Simple Shear Apparatus Capable of A Wide Range of Shear Strain Measurement," *Geotechanical Testing Journal,* Vol. 16, No. 1, pp. 3–17.

Ashmawy, A. K. and Drnevich, V. P., 1994, "A General dynamic Model for the Resonant Column/Quasi-Static Torsional Shear Apparatus," *Geotechnical Testing Journal,* Vol. 17, No. 3, pp. 337–348.

ASTM D 4015-92, 1995, "Standard Test Methods for Modulus and Damping of Soils by the Resonant-Column Method," American Society for Testing and Materials, *Annual Book of Standards,* Vol. 04.08, pp. 465–473.

Avramidis, A. S. and Saxena, S. K., 1990, "The Modified Stiffened Drnevich Resonant Column Apparatus," *Japanese Society of Soil Mechanics and Foundation Engineering,* Vol. 30, No. 3, pp. 53–68.

Cascante, G. and Santamarina, C., 1997, "Low Strain Measurements Using Random Noise Excitation," *Geotechnical Testing Journal,* Vol. 20, No. 1, pp. 29–39.

Cascante, G., Vanderkooy, J., and Chung, W., 2002, "Correction of Eddy-Current Effects on Resonant Column Measurements with a Transfer Function Model," *Canadian Geotechnical Journal* (accepted for publication).

Cascante, G., Vanderkooy, J., and Chung, W., 2003, "Difference Between Current and Voltage Measurements in Resonant-Column Testing," Canadian Geotechnical Journal (in press).

Drnevich, V. P., 1978, "Resonant-Column Problems and Solutions," *Dynamic Geotechnical Testing, ASTM STP 654,* pp. 384–398.

Drnevich, V. P., 1985, "Recent Development in Resonant Column Testing," *Proceedings,* Richart Commemorative Lectures, ASCE annual meeting, Detroit, MI, R. E. Woods, Ed., pp. 79–107.

Drnevich, V. P. and Richart, F. E., Jr., 1970, "Dynamic Prestraining of Dry Sand," *Journal of Soil Mechanics and Foundations Divisions, ASCE,* Vol. 96, No. SM2, pp. 453– 469.

Drnevich, V. P., Hardin, B. O., and Shippy, D. J., 1978, "Modulus and Damping of Soils by the Resonant-Column Method," *Dynamic Geotechnical Testing, ASTM STP 654,* pp. 91–125.

Glaser, S. D., Weiss, G., and Johnson, L. R., 1998, "Body Waves Recorded inside an Elastic Half Space by an Embedded Wideband Velocity Sensor," *Journal of the Acoustical Society of America,* Vol. 104, No. 3, pp. 1404–1412.

Hardin, B. O. and Music, J., 1965, "Apparatus for Vibration of Soil Specimens During Triaxial Test," *Instruments and Apparatus for Soil and Rock Mechanics, ASTM STP 392,* American Society for Testing and Materials, West Conshohocken, PA, pp. 55–74.

Hardin, B. O. and Richart, F. E., Jr., 1963, "Elastic Wave Velocities in Granular Soil," *Journal of the Soil Mechanics and Foundations Division, ASCE*, Vol. 89, No. SM1, pp. 33–63.

Hardin, K. O., Drnevich, V. P., Wang, J., and Sams, C. E., 1994, "Resonant Column Testing at Pressures up to 3.5 MPa (500 psi)," *Dynamic Geotechical Testing II, ASTM STP 213*, R. J. Ebelhar, V. P. Drnevich, and B. L. Kutter, B. L., Eds., pp. 222–233.

Isenhower, W. M., 1980, "Torsional Simple Shear/Resonant Column Properties of San Francisco Bay Mud," M.S. thesis, The University of Texas at Austin.

Isenhower, W. M., Stokoe, K. H., II and Allen, J. C., 1987, "Instrumentations for Torsional Shear/Resonant Column Measurements under Anisotropic Stresses," *Geotechnical Testing Journal*, Vol. 10, No. 4, pp. 183–191.

Kim, D. S., Stokoe, K. H., and Hudson, W. R., 1991, "Deformational Characteristics of Soils at Small to Intermediate Strains from Cyclic Tests," Report 1177-3, Center for Transportation Research, Bureau of Engineering Research, the University of Texas Austin.

Li, X. S., Yang, W. L., Shen, C. K., and Wang, W. C., 1998, "Energy-Injecting Virtual Mass Resonant Column System," *Journal of Geotechnical and Geoenvironmental Engineering*, Vol. 124, No. 5, pp. 428–438.

Meng, J. and Rix, G. J., 2002, "Reduction of Equipment-Generated Damping in Resonant Column Measurements," *Géotechnique*, in press.

Santamarina, J. C. and Cascante, G., 1996, "Stress Anisotropy and Wave Propagation: A Micromechanical View," *Canadian Geotechnical Journal*, Vol. 33, No. 5, pp. 770–782.

Stokoe, K. H., II, and Lodde, P. F., 1978, "Dynamic Response of San Francisco Mud," *Proceedings*, Earthquake Engineering and Soil Dynamics, ASCE, Geotechnical Engineering Division Specialty Conference, Vol. II, Pasadena, CA, June, pp. 940–959.

Wilson, S. D. and Dietrich, R. J., 1960, "Effect of Consolidation Pressure on Elastic and Strength Properties of Clay," *Proceedings*, ASCE Soil Mechanics and Foundation Division, Research Conference on Shear Strength of Cohesive Soils, Boulder, CO, ASCE, New York.

Woods, R. D., 1994, "Laboratory Measurement of Dynamic Soil Properties," *Dynamic Geotechical Testing II, ASTM STP 213*, R. J. Ebelhar, V. P. Drnevich, and B. Kutter, Eds., pp. 165–190.

Yu, P. and Richart, F. E., 1984, "Stress Ratio Effects on shear Modulus of Dry Sands," *Journal of Geotechnical Engineering, ASCE*, Vol. 110, No. 3, pp. 331–345.

Zemanek, J., Jr., and Rudnick, I., 1961, "Attenuation and Dispersion of Elastic Waves in a Cylindrical Bar," *Journal of the Acoustical Society of America*, Vol. 33, pp. 1283–1288.